Influences of the alignment and misalignment spatial filters on the beam quality in high power laser systems

2010 J. Opt. 12 095704

(http://iopscience.iop.org/2040-8986/12/9/095704)

IOP Publishing Journal of Optics
J. Opt. **12** (2010) 095704 (9pp) doi:10.1088/2040-8978/12/9/095704

Influences of the alignment and misalignment spatial filters on the beam quality in high power laser systems

Yan-Qi Gao, Bao-Qiang Zhu, Dai-Zhong Liu and Zun-Qi Lin

Shanghai Institute of Optics and Fine Mechanics, Shanghai 201800, People's Republic of China

E-mail: liufenggyq@siom.ac.cn (Y-Q Gao)

Received 4 June 2010, accepted for publication 29 July 2010
Published 23 August 2010
Online at stacks.iop.org/JOpt/12/095704

Abstract
The characteristics of the alignment and misalignment multistage spatial filters are presented in this paper based on their effects on the beam quality. First, the approximate analytical expressions of the modulations of a square beam, which are induced by scatterers and an alignment spatial filter pinhole, are derived. Then, the far field analytical expression of the modulated square beam after its propagation through a nonlinear medium is presented. Subsequently, using a square super Gaussian beam, the modulations induced by an alignment and misalignment spatial filter pinhole are illustrated. The suppressing functions of the alignment and misalignment spatial filters on the hot image are investigated. The effects of the misalignment of the multistage spatial filter pinholes on the output beam quality are studied based on two evaluation factors: fluence beam contrast and fill factor. It is shown that the spatial filter pinhole misalignment has significant influences on both the far field and near field of the downstream beam, especially when nonlinear media exist. The results presented in this paper give important references and guidance for the spatial filter design, installation and alignment.

Keywords: spatial filter, alignment, self-focusing, laser beam characterization

(Some figures in this article are in colour only in the electronic version)

1. Introduction

The spatial filter, which has become one of the most important parts of the high power laser system [1–4], was first introduced in the Cyclops laser [5] to suppress the small scaled self-focusing in 1975 [6]. It can also prevent the parasitic lasing, reduce the amplified spontaneous emission, match the beam diameter [7, 8], and suppress the hot image [9–11]. Hence, much attention has been paid to the spatial filter and its effects on improving the beam quality. Hunt studied the imaging relay function and the beam modulation caused by the spatial filter pinhole [12]. Celliers and Murray presented the performances of different shape and material pinholes based on the pinhole closure effect [13, 14]. Potemkin gave the methods to choose the shape, diameter and focal length of spatial filter lenses [7]. Garanin showed the relationship between the spatial instability rate and the mutual arrangement of nonlinear media and spatial filters [15]. However, there are few works concerning the multistage spatial filers and the impact of the misalignment spatial filters on the beam quality despite the fact that they do exist and are very important in a practical facility.

In this paper, in order to reveal the characteristics of the alignment and misalignment multistage spatial filters, the models of the scatterers, square beam modulation, and the modulation propagation through the nonlinear medium are presented in section 2. Then, the characteristics of alignment and misalignment multistage spatial filters are studied numerically based on their effects on the far field and near field beam qualities in section 3. Finally, the conclusions are outlined.

2. Modulation models in alignment spatial filter

The typical high power laser facility is composed of a chain of laser amplifiers in which spatial filters are

indispensable [16–20]. In practical system, noises induced by scattering sites, optical damage, medium nonuniformity and so on, could lead to small scale self-focusing and 'hot image' because of the nonlinear effects [21–28]. On the other hand, the diffraction effect of the flat-topped beam, which can offer a higher fill factor, could induce diffraction modulation, and it could be enhanced greatly by the nonlinear effects [29, 30]. Such instabilities limit the useful power of the solid-state laser either by creating damage or by limiting the beam focus ability. Spatial filters can remove the most dangerous high frequency components of the beam cross section, reduce the peak intensity of the 'hot image' and suppress the diffraction modulation by reducing the effective propagation length of the beam. However, the spatial filter could induce the beam modulations because of its limited band pass and misalignment [31, 32]. In this section, the approximate analytical expressions of the square beam modulations induced by the scatterers and alignment spatial filter pinhole are derived first. Then, the far field expression of the modulated square beam after its propagation through a nonlinear medium is derived. In the following calculations, the spatial filter pinhole is assumed to be a circle.

2.1. Square beam modulation induced by spatial filter pinhole

For a square beam $E(x, y) = A_0\mathrm{rect}(x/2\omega)\mathrm{rect}(y/2\omega)$, the far field intensity distribution can be written as

$$I(x, y) = A_0^2(2\omega)^4/(\lambda^2 f^2) \times \mathrm{sinc}^2(2\omega x/\lambda f)\mathrm{sinc}^2(2\omega y/\lambda f), \tag{1}$$

where ω, λ, and f are the half beam width, wavelength, and focal length of the input lens, respectively. The fractional transmission power of the square pinhole with width D_P is

$$T(D_\mathrm{P}) = \int_{-D_\mathrm{P}/2}^{D_\mathrm{P}/2}\int_{-D_\mathrm{P}/2}^{D_\mathrm{P}/2} I(u, v)\,\mathrm{d}u\,\mathrm{d}v \Big/ \int_{-\infty}^{\infty}\int_{-\infty}^{\infty} I(u, v)\,\mathrm{d}u\,\mathrm{d}v, \tag{2}$$

where $u = 2\omega x/\lambda f$, $v = 2\omega y/\lambda f$. If we write the pinhole width D_P as a factor of the diffraction limit (DL), we get $D_\mathrm{P} = N_\mathrm{P} \times 2\lambda f/2\omega$. After integral and integral transform, equation (2) becomes

$$\begin{aligned} T(N_\mathrm{P}) &= \frac{4}{\pi^2}\left[\int_0^{2N_\mathrm{P}\pi} \frac{\sin(2u)}{2u}\,\mathrm{d}(2u) - \frac{\sin^2(N_\mathrm{P}\pi)}{N_\mathrm{P}\pi}\right] \\ &\quad\times\left[\int_0^{2N_\mathrm{P}\pi} \frac{\sin(2v)}{2v}\,\mathrm{d}(2v) - \frac{\sin^2(N_\mathrm{P}\pi)}{N_\mathrm{P}\pi}\right] \\ &= \frac{4}{\pi^2}\left[\mathrm{Si}(2N_\mathrm{P}\pi) - \frac{\sin^2(N_\mathrm{P}\pi)}{N_\mathrm{P}\pi}\right]^2. \end{aligned} \tag{3}$$

For the far field of a square beam, the energies concentrate in a cross hair region mostly. Hence, equation (3) gives a good approximate expression of the fractional transmission power of a circular pinhole with diameter D_P when the pinhole is larger than several times DL and aligned with the optical axis. The modulation of the output beam induced by the spatial filter pinhole can be characterized by [12]

$$A_\mathrm{m} = [1 - T(N_\mathrm{P})]^{1/2}A_0 \qquad \lambda_\mathrm{m} = 2\omega/N_\mathrm{P}, \tag{4}$$

where A_m, λ_m, and A_0 are the modulation amplitude, the modulation scale, and the input beam amplitude, respectively. It is assumed that the focal lengths of the two lenses are both f.

2.2. Modulations induced by scatterers

Supposing that a uniform plane beam passes through a plane with scatterers, the electric intensity abutting upon the scatterer plane can be represented as

$$E(x, y) = A_0\left\{1 - \sum_{m=1}^{N_\mathrm{s}} \tau_m \exp\left[-\frac{(x - x_m)^2 + (y - y_m)^2}{2\omega_m^2}\right]\right\}, \tag{5}$$

where τ_m is the mth scatterer transmittance rate, N_s is scatterer number, and (x_m, y_m) is the mth scatterer coordinate. The scatterers are assumed to be Gaussian scatterers with waist width ω_m. Using the Collins integral formula, the far field electric intensity can be written as [33, 34]

$$\begin{aligned} E(x_2, y_2) &= -\frac{\mathrm{i}k}{2\pi B_\mathrm{s}}\int\int_{-\infty}^{+\infty} E(x, y) \\ &\quad\times \exp\left\{\frac{\mathrm{i}k}{2B_\mathrm{s}}[A_\mathrm{s}(x^2+y^2) - 2xx_2 + D_\mathrm{s}(x_2^2 + y_2^2)]\right\}\mathrm{d}x\,\mathrm{d}y, \end{aligned} \tag{6}$$

where $A_\mathrm{s} = 0$, $B_\mathrm{s} = f$, $C_\mathrm{s} = -1/f$, $D_\mathrm{s} = 1 - z_\mathrm{s}/f$, and z_s is the distance between the scatterer plane and the lens. If we ignore the background beam and just consider the scattering part, after integration and simplification, the electric intensity of the scatterers in the focal plane can be written as

$$\begin{aligned} E(x_2, y_2) &= -\frac{\mathrm{i}kA_0}{2\pi B_\mathrm{s}}\exp\left[\frac{\mathrm{i}kD_\mathrm{s}}{2B_\mathrm{s}}(x_2^2 + y_2^2)\right] \\ &\quad\times \sum_{m=1}^{N_\mathrm{s}}\left\{\frac{\pi\tau_m}{1/(2\omega_m^2) - \mathrm{i}Ak/(2B_\mathrm{s})}\exp\left(-\frac{x_m^2 + y_m^2}{2\omega_m^2}\right)\right. \\ &\quad\left.\times \exp\left[\frac{(x_m/\omega_m^2 - \mathrm{i}kx_2/B_\mathrm{s})^2}{2/\omega_m^2 - \mathrm{i}2A_\mathrm{s}k/B_\mathrm{s}} + \frac{(y_m/\omega_m^2 - \mathrm{i}ky_2/B_\mathrm{s})^2}{2/\omega_m^2 - \mathrm{i}2A_\mathrm{s}k/B_\mathrm{s}}\right]\right\}. \end{aligned} \tag{7}$$

Substituting the spatial filter parameters, equation (7) becomes

$$\begin{aligned} E(x_2, y_2) &= -\frac{\mathrm{i}kA_0}{f}\exp\left[\frac{\mathrm{i}k(1 - z_\mathrm{s}/f)}{2f}(x_2^2 + y_2^2)\right] \\ &\quad\times \sum_{m=1}^{N_\mathrm{s}}\left\{\omega_m^2\tau_m\exp\left(-\frac{x_2^2 + y_2^2}{2f^2/k^2\omega_m^2}\right)\right. \\ &\quad\left.\times \exp\left[-\frac{\mathrm{i}k}{f}(x_m x_2 + y_m y_2)\right]\right\}. \end{aligned} \tag{8}$$

Equation (8) indicates that the far field electric intensity distribution keeps the Gaussian form with beam waist $f/k\omega_m$, and the maximal electric intensity for the mth scatterer can be denoted by

$$|E_m(0, 0)| = kA_0\omega_m^2\tau_m/f. \tag{9}$$

It is also found that the far field electric field distribution has nothing to do with the longitudinal distance z_s except a phase factor. The transverse position (x_m, y_m) of the scatterer also

just affects the phase distribution. Therefore, for any scatterers with different positions, if $f/k\omega_m \ll D_P = N_P \times 2\lambda f/2\omega$, which means $\omega_m \gg \omega/(2\pi N_P)$, the suppression function of the spatial filter will be invalid. If $\omega_m \ll \omega/(2\pi N_P)$, the pinhole will be illuminated nearly uniformly. The scale of the output beam modulation in the second case can be characterized by [35]

$$2J_1(\pi N_P r/\omega)/(\pi N_P r/\omega), \tag{10}$$

where $r = [(x_2 - x_m)^2 + (y_2 - y_m)^2]^{1/2}$, and the maximal amplitude is

$$A_M = \pi^2 A_0 \tau_m \omega_m^2 N_P^2/(2\omega^2). \tag{11}$$

It is shown clearly that the scale of the scatterer modulation only depends on the pinhole parameters N_P for a given beam width ω, and the maximal amplitude is determined by the size of the scatterer ω_m, the scatterer transmittance rate τ_m, and the pinhole parameters N_P.

2.3. Modulated beam propagation through nonlinear medium

According to the Bespalov–Talanov theory [36], the solution of the linearly polarized wave equation in the form of the harmonic perturbation is

$$E = [A_0 + A_P(z)\cos(k_T x)]\exp(-ik_m \gamma |A_0|^2 z), \tag{12}$$

where the complex amplitude of the perturbation $A_P = u + iv$, k_T is the transverse wavenumber of the perturbation, k_m is the wavenumber in the nonlinear medium, $\gamma = n_2/2n_0$, n_0 and n_2 are the linear and nonlinear refractive indexes, respectively. The evolution of the perturbation in the nonlinear medium can be represented as [10]

$$A_P(z) = \begin{bmatrix} u(z) \\ v(z) \end{bmatrix} = \begin{bmatrix} \cosh(S\Theta) & -\sinh(S\Theta)/S \\ -S\sinh(S\Theta) & \cosh(S\Theta) \end{bmatrix} \times \begin{bmatrix} u(0) \\ v(0) \end{bmatrix} = M \begin{bmatrix} u(0) \\ v(0) \end{bmatrix}, \tag{13}$$

where $\Theta = k_P^2 z/(2k)$, $S = (2B/\Theta - 1)^{1/2}$, $B = k\gamma |A_0^2| z$. The transfer coefficient of amplitude perturbation is defined by $K_q(\phi) = |A_P(z)|/|A_P(0)|$, and the initial phase of the perturbation is $\phi = \arctan[v(0)/u(0)]$. For a given spatial frequency, the amplitude perturbation has the maximum transfer coefficient [15]

$$K_{max}(k_P) = \frac{B}{S\Theta}\sinh(S\Theta) + \left\{1 + \left[\frac{B}{S\Theta}\sinh(S\Theta)\right]^2\right\}^{1/2}, \tag{14}$$

when the initial perturbation phase at the input plane of the nonlinear medium equals

$$\phi_{max}^{in}(k_P) = \frac{1}{2}\left\{\frac{\pi}{2} + \arctan\left[\frac{\Theta - B}{S\Theta}\tanh(S\Theta)\right]\right\} + m\pi. \tag{15}$$

In the foregoing discussions, we have shown that the perturbations induced by limited band pass, suppressed scatterers and unsuppressed scatterers are all low spatial frequencies. Hence, equation (14) can be approximately replaced by [15]

$$K_{max} \approx B + (1 + B^2)^{1/2}, \tag{16}$$

and we get

$$|A_P(z)| = |A_P(0)| \times [B + (1 + B^2)^{1/2}]. \tag{17}$$

In the Bespalov–Talanov theory which is based on the plane wave approximation, the limited beam breadth is not considered. Usually, the length of the nonlinear medium is short and the Rayleigh length is long enough, so the diffraction effect can be ignored approximately. A modulated rectangle beam propagation through a nonlinear medium with length z can be simply represented by

$$E_Z(x) = \mathrm{rect}\left(\frac{x}{2\omega}\right)[A_0 + A_P(z)\cos(k_T x)]. \tag{18}$$

The electric intensity distribution in the focal plane of the spatial filter is

$$E_P(x) = A_0 \frac{2\omega}{\sqrt{\lambda f}}\mathrm{sinc}\left(\frac{2\omega}{\lambda f}x\right) + A_P(z)\frac{\omega}{\sqrt{\lambda f}}\mathrm{sinc}\left[\frac{2\omega}{\lambda f}(x - k_T)\right] + A_P(z)\frac{\omega}{\sqrt{\lambda f}}\mathrm{sinc}\left[\frac{2\omega}{\lambda f}(x + k_T)\right]. \tag{19}$$

Equation (19) shows that the electric intensities of the side lobes are directly proportional to the modulation transfer coefficient K_{max}, and the shapes of them are similar to the main lobe. The position of the side lobe is decided by the transverse wavenumber k_T. If the k_T is big enough and the side lobe intensity is small, it is easy to be cut off. But when the k_T is small and the side lobe intensity is strong, a cutoff of the side lobe would affect the intensity distribution of the output beam.

The above results, which are based mostly on [10, 12, 15, 34–36], give the simple reasonable approximate models of dominating factors of the single alignment spatial filter. But they are far from enough for spatial filter design, installation and alignment in high power laser systems. It is very hard to get the simple analytical expression of the far field and near field intensity distributions of a shaped beam in multistage spatial filters, especially in the misalignment multistage spatial filters. Hence, we will present the characteristics of this system based on the above analyses and numerical methods in section 3.

3. Simulation of the alignment and misalignment multistage spatial filters

The approximate models for the scatterers, modulations and modulation propagations in the single alignment spatial filter with nonlinear medium have been built in section 2. In this section, the above models, the Fresnel diffraction integral [35], and the split-step Fourier method (STFM) [37, 38] are applied to investigate the characteristics of the alignment

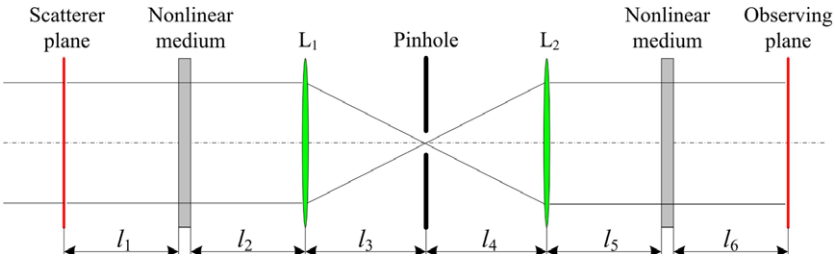

Figure 1. Schematic diagram of one stage of the multistage spatial filter with nonlinear media.

and misalignment multistage spatial filters. In the following calculations, the 30th order super Gaussian beam is used, the beam width is 5 cm, the wavelength is 1053 nm, and the focal lengths of all the lenses are 1 m. The area of the sampling region is 10 cm × 10 cm, and is divided into 512 × 512 grid points unless specially mentioned.

3.1. Beam modulation induced by limited pinhole diameter

One of the most important problems, which we meet when the spatial filter is used in the high power laser system, is the output beam modulation induced by limited pinhole bandwidth. Equations (3) and (4) give the approximate expressions of the amplitude and the period of modulation induced by the alignment spatial filter. It is noticed that equations (3) and (4) are obtained based on the rectangular beam profile. However, the beam profile used in the high power laser systems is often shaped in order to suppress the diffraction rings [30]. The super Gaussian beam is one kind of such beam. Because the edge of the super Gaussian beam is no longer as sharp as the rectangular one, the amplitude of the modulation induced by the limited band pass decreases. Hence, the modulation amplitude A_{m} in equation (4) can be thought as the worst situation of this modulation. The modulation scale λ_{m} in equation (4) gives a good approximate expression of the modulation period. But it is just helpful when the spatial filter is aligned.

As a practical example, figure 2 presents the modulations induced by the alignment and misalignment spatial filters when the pinhole sizes are 8 × DL. In this section, the nonlinear medium is not included. The input beam locates on the front focal plane of the first spatial filter lens, and the observing plane locates on the back focal plane of the second lens. From the first two curves in figure 2(a), we can find that the modulation amplitude of the rectangular beam is obviously larger than the super Gaussian beam. The last four curves present the evolution of the modulation with the increment of the pinhole transverse offset (TO). The energy of the low frequency components is much bigger than that of the high frequency components, so the modulation exhibits the low frequency characteristics and the modulation frequency decreases. But the shape of the modulation becomes irregular owing to the other side of the higher frequency components in the focal plane passing though the offset pinhole. Figure 2(b) shows the propagation characteristics of the modulated beam in free space when the transverse offset is $0.2 \times D_{\mathrm{P}}$. The propagation length L indicates the distance between the observing plane and the back focal plane of the second lens with unit 'm'. It is found that one side of the output beam (the left side in figure 2(b)) becomes smooth, and the other side of the output beam (the right side) becomes sharper as the propagation distance increases. Figure 3 gives some typical modulations and their propagations when the distance between pinhole and confocal plane (DPF) is $0.3\% \times f$ and the pinhole locates after the confocal plane in (a)–(c), the DPF is $0.5\% \times f$ and the pinhole locates before the confocal plane in (d)–(f). The transverse offset of the pinhole is $0.1 \times D_{\mathrm{P}}$ in (b), (c), (e), (f) and 0 in (a), (d). It shows that not only the modulations but also the whole beam shapes are disturbed by the misalignment pinhole seriously. These modulations are one of the seeds of nonlinear increase. The characteristics of different modulation shapes also offer a useful way to estimate the relative position of the pinhole and the lens, and meanwhile, they provide a novel beam shaping method [39].

3.2. Beam modulation induced by scatterers

Because the modulation induced by scatterers can form a hot image when they propagate through a nonlinear medium [9–11], the modulation characteristics are very important and interesting. In section 2, it is shown that the spatial filter cannot suppress the scatterers when $\omega_m \gg \omega/(2\pi N_{\mathrm{P}})$, and the modulations have the same characteristics which can be denoted by equations (10) and (11) when $\omega_m \ll \omega/(2\pi N_{\mathrm{P}})$. Because the focal spot is either small enough or big enough for the above two situations, the differences between the modulations induced by the alignment spatial filter and those induced by the misalignment spatial filter are not obvious. But when the scatterer size is close to $\omega/(2\pi N_{\mathrm{P}})$, the misalignment spatial filter will disturb the modulations obviously. In this section, the numerical simulations are based on a simple system as shown in figure 1. We assume that the length of the first nonlinear medium is zero (this first nonlinear medium does not exist), $l_1 = l_2 = l_3 = l_4 = l_5 = 1$ m, the length of the second nonlinear medium is 30 cm, the linear and nonlinear refractive indices $n_0 = 1.53$ and $n_2 = 1.29 \times 10^{-22}$ m^2 W^{-1}, the radiation intensity is 3 GW cm^{-2}, and the scatterer locates on the centre of the beam with $\tau_m = 1$.

Figure 4 shows the output beam cross section of this system when $l_6 = 0.91$ m, which is decided by the position of the hot image, and the scatterer sizes ω_m are $0.8 \times \omega/(2\pi N_{\mathrm{P}})$, $\omega/(2\pi N_{\mathrm{P}})$ and $1.2 \times \omega/(2\pi N_{\mathrm{P}})$, respectively. The small figure is one part of its corresponding figure. The three kinds of lines indicate the situations when there is no pinhole in the focal

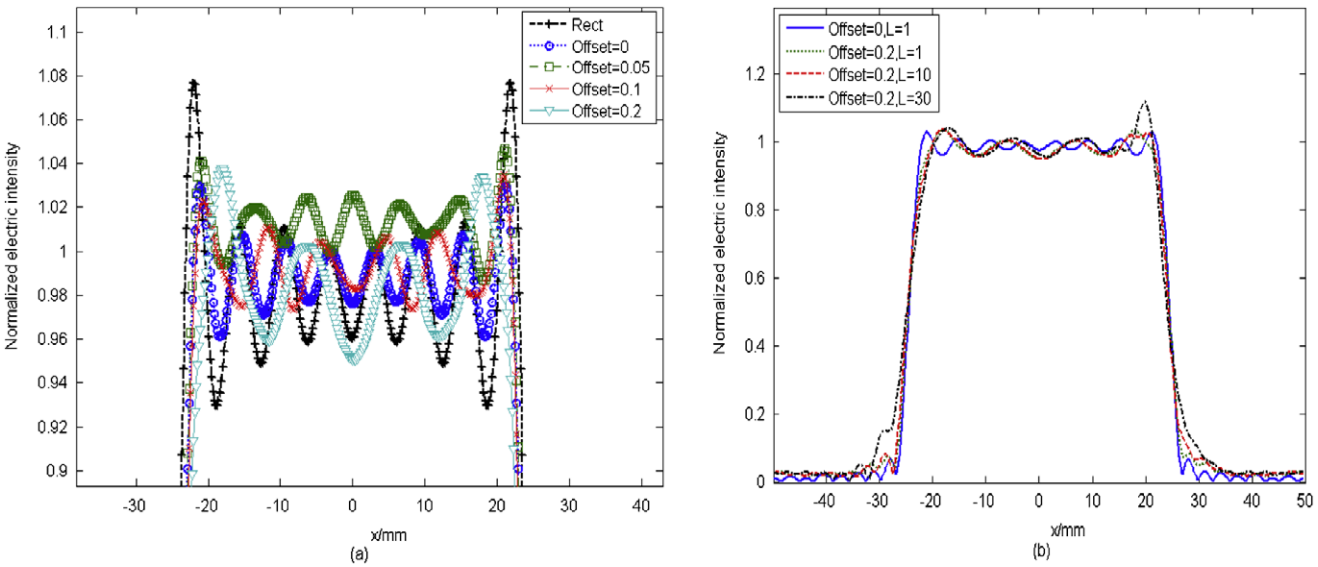

Figure 2. Modulations induced by a spatial filter when the pinhole size is $N_p = 8$: (a) modulations induced by different TO, (b) propagation characteristics of the modulations when TO is $0.2 \times D_P$.

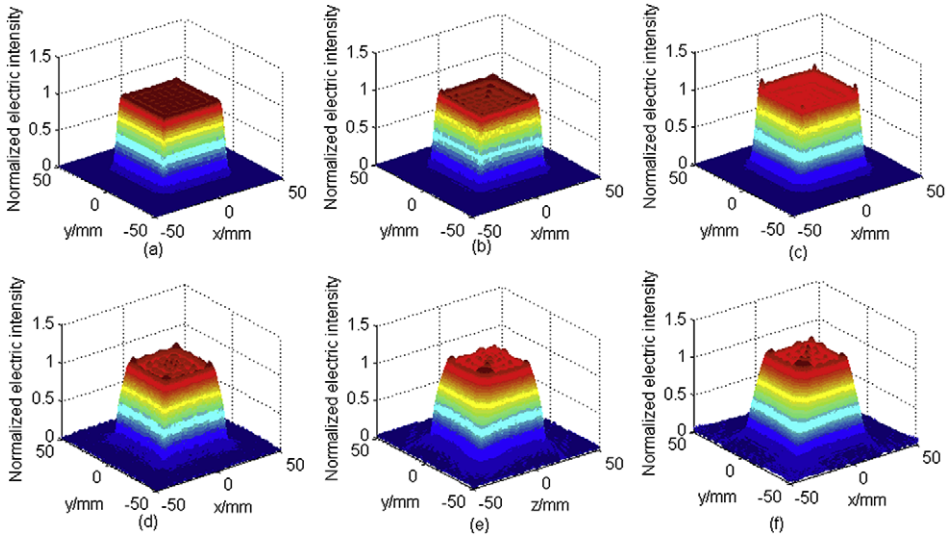

Figure 3. Modulations induced by the misalignment spatial filter when the pinhole does not locate on the confocal plane and $N_p = 10$. The DPF is $0.3\% \times f$ and the pinhole locates after the confocal plane in (a)–(c). The DPF is $0.5\% \times f$ and the pinhole locates before the confocal plane in (d)–(f). The TO is 0 in (a), (d), and it is $0.1 \times D_P$ in (b), (c), (e), (f). The distance between the observed plane and the output lens is $20 \times f$ in (c), (f), and it is f in other figures.

plane, the pinhole size is $30 \times$ DL without offset, and $30 \times$ DL with transverse offset $0.1 \times D_P$, respectively. The reason why $30 \times$ DL is chosen is to avoid the serious disturbance induced by the pinhole and observe modulation characteristics of the scatterers easily. Figure 4 indicates that the spatial filter can suppress the hot image greatly. Because of the pinhole, the peak intensity is reduced to about 1.1 while it is almost 6 when the spatial filter pinhole is absent in this experiment. Comparing the second curve with the third cove in each small figure, we can find that the modulation peaks induced by the misalignment pinhole are about twice those induced by the alignment pinhole. The modulations, which are dangerous sources of the downstream nonlinear increment, induced by the misalignment pinhole spread to the whole beam, and they are irregular. The suppressing function of the spatial filter for the hot image can be explained by on one hand the limited band pass of the spatial filter pinhole cutting off the higher frequencies of the 'Fresnel-zone', and on the other hand the low frequency modulation induced by the spatial filter pinhole disturbing the passed low frequency 'Fresnel-zone'. Hence, the above two points should be considered when choosing the pinhole size for suppressing the hot image.

3.3. Multistage spatial filters

Because of the employment of the flat-topped beam and image relay, the influence of the whole beam self-focusing can be ignored [12]. The main factors, which could induce focal spot degradation, are the beam modulations induced by pinholes and scatterers, and their nonlinear propagation in

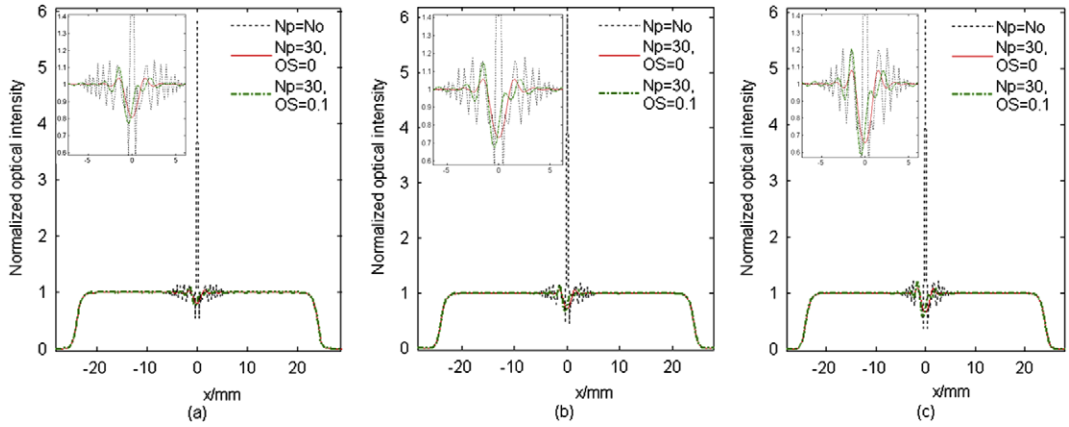

Figure 4. Hot image induced by a scatterer with and without a spatial filter, the small figure is a part of its corresponding figure, the scatterer size is $0.8 \times \omega/(2\pi N_{\mathrm{P}})$ (a), $\omega/(2\pi N_{\mathrm{P}})$ (b), and $1.2 \times \omega/(2\pi N_{\mathrm{P}})$ (c).

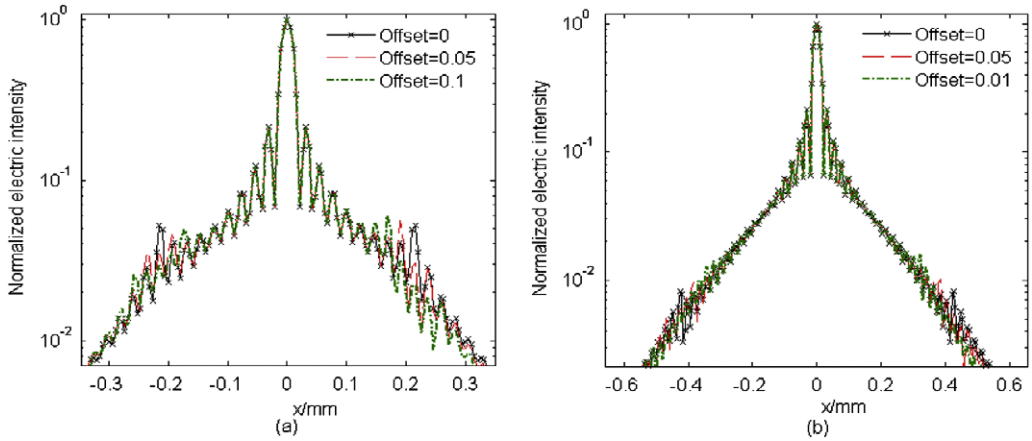

Figure 5. Normalized electric intensity distribution in the CSF focal plane when the size of the PSF pinhole is 10 × DL (a), and 20 ×DL (b), three kinds of curves denote the focal spots with TO 0, $0.05 \times D_{\mathrm{P}}$, and $0.1 \times D_{\mathrm{P}}$, respectively.

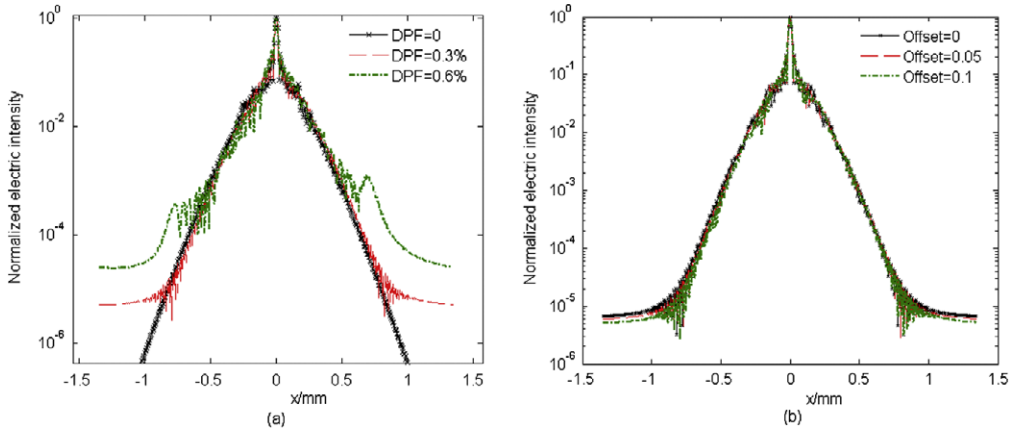

Figure 6. Normalized electric intensity distribution in the CSF focal plane, (a) TO is $0.1 \times D_{\mathrm{P}}$, DPL are 0, $0.3\% \times f$, and $0.6\% \times f$, respectively, (b) the DPF is $0.3\% \times f$, TO is 0, $0.05 \times D_{\mathrm{P}}$, and $0.1 \times D_{\mathrm{P}}$ respectively.

the downstream systems (the blemishes and machine errors of elements are not involved here). The far field and near field degradations, which are induced by the beam modulations and their nonlinear propagations, are investigated in this section. The configuration used in the following calculations is composed of two parts: the first spatial filter system and the second spatial filter system. The first spatial filter system includes a spatial filter and a nonlinear medium with a length of 30 cm, whose front surface locates on the back focal plane of the output lens. It is called the prestage spatial filter (PSF). The second spatial filter system, which is called the current spatial filter (CSF), is the same as the prestage spatial filter. The back

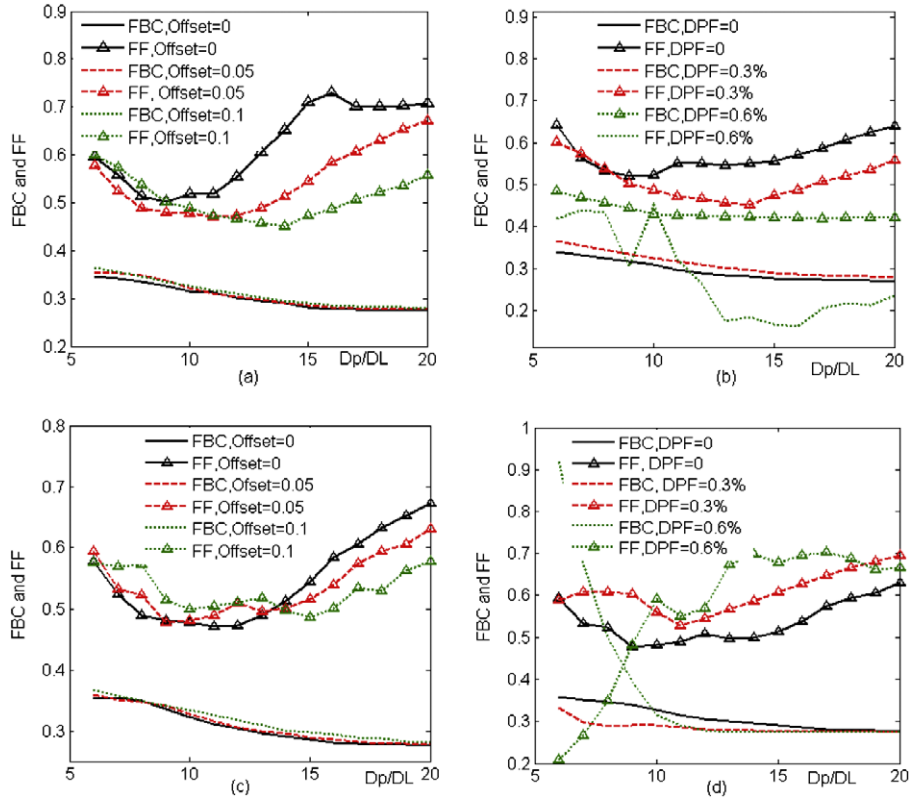

Figure 7. FBC and FF with different pinhole offsets and pinhole sizes, (a) the PSF pinhole has a DPF $0.3\% \times f$ and a transverse offset 0, $0.05 \times D_{\mathrm{P}}$, and $0.1 \times D_{\mathrm{P}}$, (b) the PSF pinhole has a TO $0.1 \times D_{\mathrm{P}}$, and a DPF 0, $0.3\% \times f$, and $0.6\% \times f$, the CSF pinhole is aligned in (a) and (b). The TO is $0.05 \times D_{\mathrm{P}}$ and the DPF is $0.3\% \times f$ for the PSF pinhole in (c) and (d). The DPF of the CSF pinhole is 0 and TO is 0, $0.05 \times D_{\mathrm{P}}$, and $0.1 \times D_{\mathrm{P}}$ in (c), and the TO is $0.05 \times D_{\mathrm{P}}$, the DPF is 0, $0.3\% \times f$, and $0.6\% \times f$ in (d).

surface of the first nonlinear medium locates on the front focal plane of the current spatial filter. The input beam locates on the front focal plane of the prestage spatial filter. Other parameters are the same as those in section 3.2.

In order to show the far field characteristics clearly, the sampling region is extended to 20 cm × 20 cm and the grid points are not changed in figures 5 and 6. Figure 5 presents the normalized electric intensity distributions in the current spatial filter focal plane when the pinhole sizes of the prestage spatial filter are 10 × DL and 20 × DL, respectively. The y-axes are plotted in logarithmic coordinates. It is shown that the frequency components near the cutoff frequency of the prestage spatial filter are enhanced when the transverse offset is 0. It corresponds with that predicted by the B–T theory in section 2. But the amplitude is much smaller than that obtained by equation (19). This is because equation (19) is derived when the perturbation phase satisfies equation (15). In other words, it is the worst case. The transverse offset of the prestage spatial filter pinhole induces two different cutoff frequencies in each side of the focal plane. Hence, the two frequencies and those between them are amplified when the beam propagates through the nonlinear medium, as shown in figure 5 (the last two curves). Figure 6 presents the normalized electric intensity distribution in the current spatial filter focal plane when the pinhole of the prestage spatial filter has both the transverse offset and the axial offset (DPF). We can find that the frequency components become complicated and the amplitudes of the higher frequency components increase as the axial offset DPF increases. It is very dangerous for the downstream nonlinear propagation.

Subsequently, the near field beam quality of the output beam is evaluated by the fluence beam contrast (FBC) and fill factor (FF) [16]. The FBC, which is given by equation (1) in [16], is defined as the standard deviation of the fluence divided by its mean value. The FF is defined as the ratio of the average intensity to the peak intensity. In the following calculations, the prestage spatial filter pinhole size is 10 × DL.

Figure 7 shows the FBCs and FFs when the prestage spatial filter pinhole offsets and current spatial filter pinhole sizes are different. (a) and (b) are those when the current spatial filter pinhole is aligned and the prestage spatial filter pinhole is misaligned. (c) and (d) indicate the FBCs and FFs with different current spatial filter pinhole offset when the prestage spatial filter pinhole transverse offset is $0.05 \times D_{\mathrm{P}}$ and axial offset DPF is $0.3\% \times f$. The abscissa is the size of the current spatial filter pinhole which is denoted by the ×DL. It is well known that the smaller the pinhole is, the better the suppressing effect is for the small scale self-focusing. But the smaller pinhole would induce stronger modulation because of cutoff. In the multistage spatial filters, the choice of current spatial filter pinhole size is also restricted by the prestage spatial filter pinhole size and its alignment tolerance. As shown in figure 7, the FF is the smallest, which means the peak intensity of the output beam is the highest, when the

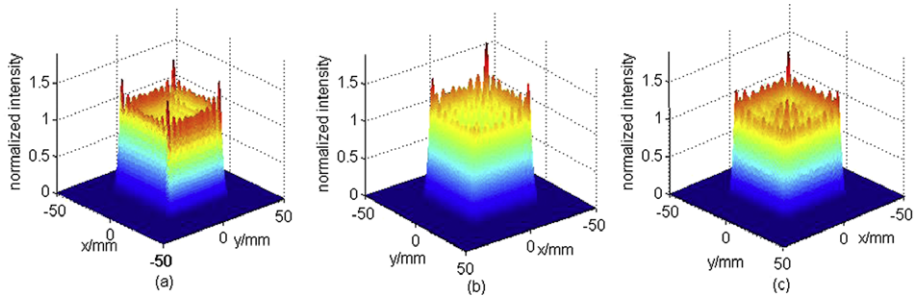

Figure 8. Typical output beam of this system when the PSF and CSF pinhole sizes are both 10 × DL, (a) the PSF and CSF pinholes are aligned, (b) the TO and DPF of the PSF pinhole are 0.05 × D_P, 0.3% × f, respectively, and the TO of the CSF is 0.05 × D_P, (c) the TO and DPF of the PSF pinhole are 0.05 × D_P, 0.3% × f and the those of the current spatial filter are 0.05 × D_P, 0.3% × f.

current spatial filter pinhole size is near the prestage spatial filter pinhole size (black line). The smallest point moves toward the bigger pinhole size direction (corresponding to a higher frequency component) as the misalignment parameter increases. This can be explained by the misalignment pinhole of the prestage spatial filter being able to enhance the high frequency components of its output beam (as shown in figures 5 and 6). When these components just locate near the edge of the current spatial filter pinhole, they will be amplified during propagation through the nonlinear medium. Therefore, the choice of the current spatial filter pinhole size should avoid the frequency components induced by the prestage spatial filter pinhole and their misalignment. For the transverse offset, it can be calculated by $(1 \pm \mathrm{OF})D_P$, where OF is the transverse offset of the prestage spatial filter pinhole. But it is too hard to give a simple analytical expression when both the transverse and axial offset present, and the numeric method is needed. If the axial offset DPF is too large, the output beam would be disturbed badly as shown in figures 6(b) and (d) (dotted line). Figure 8 illustrates three typical modulated beams induced by the multistage misaligned spatial filters and amplified by nonlinear media when both the prestage spatial filter and current spatial filter pinhole sizes are 10 × DL.

The results shown in this section also provide insight into the parameter choice in high power laser system design, such as the alignment parameters, assembly parameters and adjustment parameters.

4. Conclusions

In this paper, we first present the approximate analytical expression of the modulations induced by the alignment spatial filter pinhole and scatterers. The far field electric intensity distribution of the modulated square beam propagation through a nonlinear medium is derived approximately. Based on the Fourier diffraction integral, the STFM and the above analytical expressions, the propagation characteristics of the 30th order super Gaussian beam through alignment and misalignment multistage spatial filters with nonlinear media are illustrated. Results show that both the transverse offset and the axial offset of the spatial filter pinhole have significant influence on the output beam quality, especially when these two kinds of offsets present at the same time. The results provide useful reference and guidance for the spatial filter alignment and multistage spatial filter pinhole choice.

Acknowledgments

This work was supported by the National High Technology Research and Development Program of China (Grant No. 007SQ804), the Japan–Korea–China Cooperative Project on High Energy Density Science for Laser Fusion Energy, and the Large Scientific Facilities maintenance and upgrade of CAS.

References

[1] Hogan W J, Moses E I, Warner B E, Sorem M S and Soures J M 2001 The national ignition facility *Nucl. Fusion* **41** 567–73
[2] Waxer L J *et al* 2005 High-energy petawatt capability for the omega laser *Opt. Photonics News* **16** 30–6
[3] Fleurot N, Cavailler C and Bourgade J L 2005 The laser Mégajoule (LMJ) project dedicated to inertial confinement fusion: development and construction status *Fusion Eng. Des.* **74** 147–54
[4] Dunne M 2006 A high-power laser fusion facility for Europe *Nat. Phys.* **2** 2–5
[5] Glaze J A 1975 High energy glass lasers *Opt. Eng.* **15** 136–42
[6] Simmons W W, Hunt J T and Warren W E 1981 Light propagation through large laser systems *IEEE J. Quantum Electron.* **17** 1727–44
[7] Potemkin A K, Barmashova T V, Kirsanov A V, Martyanov M A, Khazanov E A and Shaykin A A 2007 Spatial filters for high-peak-power multistage laser amplifiers *Appl. Opt.* **46** 4423–30
[8] Gao Y Q, Zhu B Q, Liu D Z, Liu X F and Lin Z Q 2009 Characteristics of beam alignment in a high power four-pass laser amplifier *Appl. Opt.* **48** 1591–7
[9] Peng T, Zhao J L, Xie L P, Ye Z J, Wei H H, Su J Q and Zhao J P 2007 Simulation analysis of the restraining effect of a spatial filter on a hot image *Appl. Opt.* **46** 3205–9
[10] Hunt J T, Manes K R and Renard P A 1993 Hot images from obscurations *Appl. Opt.* **32** 5973–82
[11] Xie L P, Jing F, Zhao J L, Su J Q, Wang W Y and Peng H S 2004 Nonlinear hot-image formation of an intense laser beam in media with gain and loss *Opt. Commun.* **236** 343–8
[12] Hunt J T, Glaze J A, Simmons W W and Renard P A 1978 Suppression of self-focusing through low-pass spatial filtering and relay imaging *Appl. Opt.* **17** 2053–7
[13] Celliers P M, Estabrook K G, Wallace R J, Murray J E, Da Silva L B, MacGowan B J, Van Wonterghem B M and Manes K R 1998 Spatial filter pinhole for high-energy pulsed lasers *Appl. Opt.* **37** 2371–8

[14] Murray J E, Milam D, Boley C D, Estabrook K G and Caird J A 2000 Spatial filter pinhole development for the national ignition facility *Appl. Opt.* **39** 1405–20
[15] Garanin S G, Epatko I V, L'vov L V, Serov R V and Sukharev S A 2007 Self-focusing suppression in a system of two nonlinear media and a spatial filter *Quantum Electron.* **37** 1159–65
[16] Haynam C A *et al* 2007 National ignition facility laser performance status *Appl. Opt.* **46** 3276–303
[17] Baker K L, Homoelle D, Utternback E, Stappaerts E A, Siders C W and Barty C P J 2009 Interferometric adaptive optics testbed for laser pointing, wavefront control and phasing *Opt. Express* **17** 16696–709
[18] Moses E I, Boyd R N, Remington B A, Keane C J and Al-Ayat R 2009 The national ignition facility: ushering in a new age for high energy density science *Phys. Plasmas* **16** 041006
[19] Potemkin A K, Khazanov E A, Martyanov M A and Kochetkova M S 2009 Compact 300 J/300 GW frequency-doubled neodymium glass laser-part I: limiting power by self-focusing *IEEE J. Quantum Electron.* **45** 336–44
[20] Poteomkin A K, Khazanov E A, Martyanov M A, Kirsanov A V and Shaykin A A 2009 Compact 300 J/300 GW frequency-doubled neodymium glass laser-part II: description of laser setup *IEEE J. Quantum Electron.* **45** 854–62
[21] Bliss E S, Hunt J T, Renard P A, Sommargren G E and Weaver H J 1976 Effects of nonlinear propagation on laser focusing properties *IEEE J. Quantum Electron.* **12** 402–6
[22] Fibich G and Gaeta A L 2000 Critical power for self-focusing in bulk media and in hollow waveguides *Opt. Lett.* **25** 335–7
[23] Feit M D and Fleck J A Jr 1988 Beam nonparaxiality, filament formation, and beam breakup in the self-focusing of optical beams *J. Opt. Soc. Am.* B **5** 633–40
[24] Villate D, Blanchot N and Rouyer C 2007 Beam breakup integral measurement on high-power laser chains *Opt. Lett.* **32** 524–6
[25] Fleck J A, Morris J R and Bliss E S 1978 Small-scale self-focusing effects in a high power glass laser amplifier *IEEE J. Quantum Electron.* **14** 353–63
[26] Suydam B R 1975 Effect of refractive index nonlinearity on the optical quality of high-power laser beams *IEEE J. Quantum Electron.* **11** 225–30
[27] Li D, Zhao J, Peng T and Cai Z 2009 Theoretical analysis of the image with a local intensity minimum during hot image formation in high-power laser systems *Appl. Opt.* **48** 6229–33
[28] Ye Z J, Zhao J L, Peng T and Li D 2009 Evolution of the hot image effect in high-power laser system with cascaded Kerr medium *Opt. Lasers Eng.* **47** 1199–204
[29] Grow T D, Ishaaya A A, Vuong L T, Gaeta A L, Gavish N and Fibich G 2006 Collapse dynamics of super-Gaussian beams *Opt. Express* **14** 5468–75
[30] Auerbach J M and Karpenko V P 1994 Serrated-aperture apodizers for high-energy laser systems *Appl. Opt.* **33** 3179–83
[31] Awwal A A S, Rice K L and Taha T M 2009 Hardware accelerated optical alignment of lasers using beam-specific matched filters *Appl. Opt.* **48** 5190–6
[32] Candy J V, McClay W A, Awwal A A S and Ferguson S W 2005 Optimal position estimation for the automatic alignment of a high-energy laser *J. Opt. Soc. Am.* A **22** 1348–56
[33] Gao Y Q, Zhu B Q, Liu D Z and Lin Z Q 2009 Propagation of flat-topped multi-Gaussian beams through an apertured ABCD optical system *J. Opt. Soc. Am.* A **26** 2139–46
[34] Gao Y, Zhu B, Liu D and Lin Z 2009 Propagation of flat-topped multi-Gaussian beams through a double-lens system with apertures *Opt. Express* **17** 12753–66
[35] Goodman J W 2005 *Introduction to Fourier Optics* (Englewood, CO: Roberts & Co.)
[36] Bespalov V I and Talanov V I 1966 Filamentary structure of light beams in nonlinear liquids *JETP Lett.* **3** 307–10
[37] Burzler J M, Hughes S and Wherrett B S 1996 Split-step Fourier methods applied to model nonlinear refractive effects in optically thick media *Appl. Phys.* B **62** 389–97
[38] Bergé L, Gouédard C, Schjødt-Eriksen J and Ward H 2003 Filamentation patterns in Kerr media versus beam shape robustness, nonlinear saturation and polarization states *Physica* D **176** 181–211
[39] Liu Z J, Zhao H F, Liu J L, Lin J, Ahmad M A and Liu S T 2007 Generation of hollow Gaussian beams by spatial filtering *Opt. Lett.* **32** 2076–8